JACC: BASIC TO TRANSLATIONAL SCIENCE VOL. 3, NO. 3, 2018

PRECLINICAL RESEARCH

In Vivo Reactive Oxygen Species Detection With a Novel Positron Emission Tomography Tracer, ^{18}F-DHMT, Allows for Early Detection of Anthracycline-Induced Cardiotoxicity in Rodents

Nabil E. Boutagy, PhD,[a,*] Jing Wu, PhD,[b,*] Zhengxi Cai, PhD,[b] Wenjie Zhang, PhD,[b,c] Carmen J. Booth, DVM, PhD,[d] Tassos C. Kyriakides, PhD,[e] Daniel Pfau, BS,[a] Tim Mulnix, PhD,[b] Zhao Liu, PhD,[a] Edward J. Miller, MD, PhD,[a] Lawrence H. Young, MD,[a] Richard E. Carson, PhD,[b] Yiyun Huang, PhD,[b] Chi Liu, PhD,[b] Albert J. Sinusas, MD[a,b]

VISUAL ABSTRACT

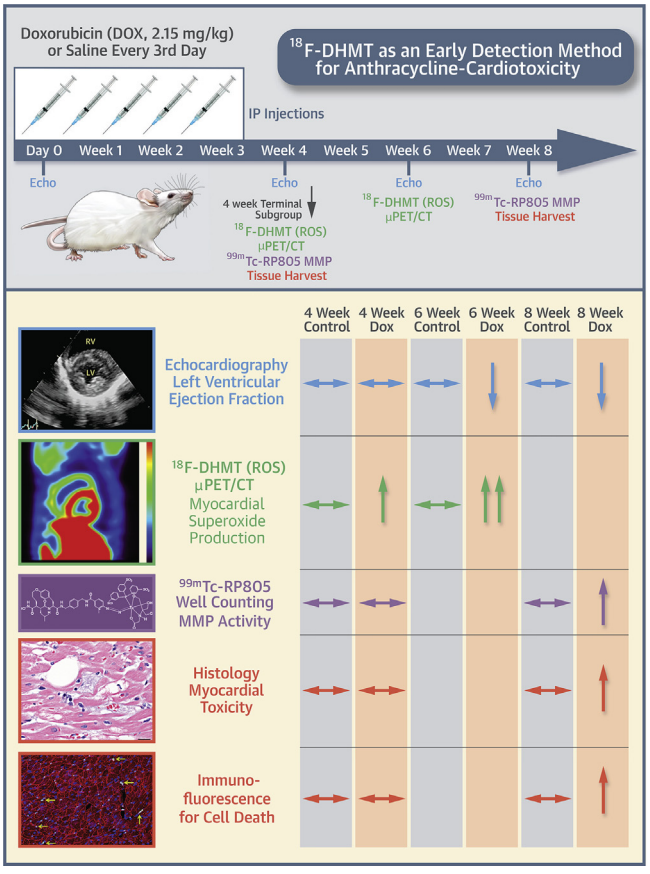

Boutagy, N.E. et al. J Am Coll Cardiol Basic Trans Science. 2018;3(3):378–90.

HIGHLIGHTS

- **LVEF is used to detect doxorubicin-induced cardiotoxicity in patients, but this index is variable and has limited ability to detect early cardiotoxicity.**
- **Doxorubicin induces cardiotoxicity largely through the excessive production of ROS.**
- **We hypothesized that ^{18}F-DHMT, a PET tracer that detects superoxide production, would provide an early index of cardiotoxicity in rodents.**
- **^{18}F-DHMT PET imaging was able to detect an elevation in cardiac superoxide production before a fall in LVEF.**
- **The early elevation in myocardial superoxide production was associated with only mild myocardial toxicity and occurred before cellular apoptosis or significant activation of MMPs; enzymes associated with myocardial remodeling.**
- **A drop in LVEF was associated with a significant increase in MMP activation, cellular apoptosis, and significant myocardial toxicity.**

ISSN 2452-302X https://doi.org/10.1016/j.jacbts.2018.02.003

SUMMARY

Reactive oxygen species (ROS) are involved in doxorubicin-induced cardiotoxicity. The authors investigated the efficacy of ^{18}F-DHMT, a marker of ROS, for early detection of doxorubicin-induced cardiotoxicity in rats. Echocardiography was performed at baseline and 4, 6, and 8 weeks post-doxorubicin initiation, whereas in vivo superoxide production was measured at 4 and 6 weeks with ^{18}F-DHMT positron emission tomography. Left ventricular ejection fraction (LVEF) was not significantly decreased until 6 weeks post-doxorubicin treatment, whereas myocardial superoxide production was significantly elevated at 4 weeks. ^{18}F-DHMT imaging detected an elevation in cardiac superoxide production before a fall in LVEF in rodents and may allow for early cardiotoxicity detection in cancer patients. (J Am Coll Cardiol Basic Trans Science 2018;3:378–90) © 2018 The Authors. Published by Elsevier on behalf of the American College of Cardiology Foundation. This is an open access article under the CC BY-NC-ND license (http://creativecommons.org/licenses/by-nc-nd/4.0/).

ABBREVIATIONS AND ACRONYMS

2D = 2-dimensional
CT = computed tomography
DOX = doxorubicin HCl
H&E = hematoxylin and eosin
LV = left ventricle/ventricular
LVEF = left ventricular ejection fraction
MMP = matrix metalloproteinase
MT = Masson's trichrome
PET = positron emission tomography
ROS = reactive oxygen species
SUV = standardized uptake value
TUNEL = terminal deoxynucleotidyl transferase-mediated nick-end labeling
VOI = volume of interest

Doxorubicin (DOX) (Adriamycin) is a widely used antineoplastic agent of the anthracycline drug class that is effective against solid tumors and hematologic malignancies (1). Although effective, a common side effect of DOX therapy is cardiotoxicity, which affects 3% to 26% of patients and often manifests as heart failure (1,2). DOX-induced cardiotoxicity is largely dose-dependent, thus limiting the use of this agent and optimal oncological treatment (3). Current guidelines to detect DOX-induced cardiotoxicity are based on the serial assessment of global systolic function. Generally, the left ventricular (LV) ejection fraction (LVEF) is assessed by nuclear gated blood pool studies or cardiac ultrasound (4). However, assessment of LVEF is variable and has limited ability to detect early cardiotoxicity, as many patients have histological evidence of cardiotoxicity before decrements in systolic function occur (5). Importantly, a reduction in LVEF is often an irreversible side effect of DOX therapy, as 45% to 58% do not recover systolic function despite receiving optimal medical therapy (6). As such, early detection methods of anthracycline-induced cardiotoxicity that precede decrements in LVEF have been proposed (6–10); however, limited or inconsistent data exist regarding the efficacy of these approaches (4).

The precise mechanisms of DOX-induced cardiotoxicity are not fully elucidated; although it is well established that DOX induces cardiotoxicity largely through the excessive production of reactive oxygen species (ROS) that lead to direct myocardial apoptosis, contractile abnormalities, inflammation, and vascular injury (11,12), and promote deleterious cardiac remodeling by increasing the activity and abundance of matrix metalloproteinases (MMPs) (13,14). Some studies report that elevations in circulating biomarkers of oxidative stress (myeloperoxidase) precede clinically significant systolic dysfunction in anthracycline-treated patients (8,15). However, the signal-to-noise ratio for cardiac-specific detection of ROS with circulating oxidative stress biomarkers may be low considering that DOX induces oxidative stress in extracardiac organs (e.g., liver, skeletal muscle) (16,17), and tumor cells can also produce

From the [a]Section of Cardiovascular Medicine, Department of Medicine, Yale Translational Research Imaging Center, Yale School of Medicine, New Haven, Connecticut; [b]Department of Radiology and Biomedical Imaging, Yale School of Medicine, New Haven, Connecticut; [c]Department of Nuclear Medicine, West China Hospital of Sichuan University, Chengdu, China; [d]Section of Comparative Medicine, Yale School of Medicine, New Haven, Connecticut; and the [e]Yale School of Public Health (Biostatistics), Yale School of Medicine, New Haven, Connecticut. This study was supported by National Institutes of Health grants R01HL123949 (Dr. C. Liu), R01HL113352 (Dr. Sinusas), T32HL098069 (Dr. Sinusas), and S10OD010322 (Dr. Carson). Dr Miller has received grant funding from Bracco, Inc. for FDG-PET examinations in cardiac sarcoidosis unrelated to the present study; and is a consultant for GE, Bracco, Inc., and Alnylam. Dr. Young has received research grant support, unrelated to this study, from Merck, Mifcor, and Novartis (to Yale University); and has as served as a consultant for Portage. Dr. C. Liu has had research contracts with GE Healthcare, Siemens Medical Solutions, and Philips Healthcare. Dr. Sinusas is a paid consultant and limited partner of MicroVide, LLC, which holds patents related to Tc99m-RP805 imaging in heart failure. All other authors have reported that they have no relationships relevant to the contents of this paper to disclose. *Drs. Boutagy and Wu contributed equally to this work.
All authors attest they are in compliance with human studies committees and animal welfare regulations of the authors' institutions and Food and Drug Administration guidelines, including patient consent where appropriate. For more information, visit the *JACC: Basic to Translational Science* author instructions page.

Manuscript received August 14, 2017; revised manuscript received February 6, 2018, accepted February 9, 2018.

FIGURE 1 Schematic of Experimental Design

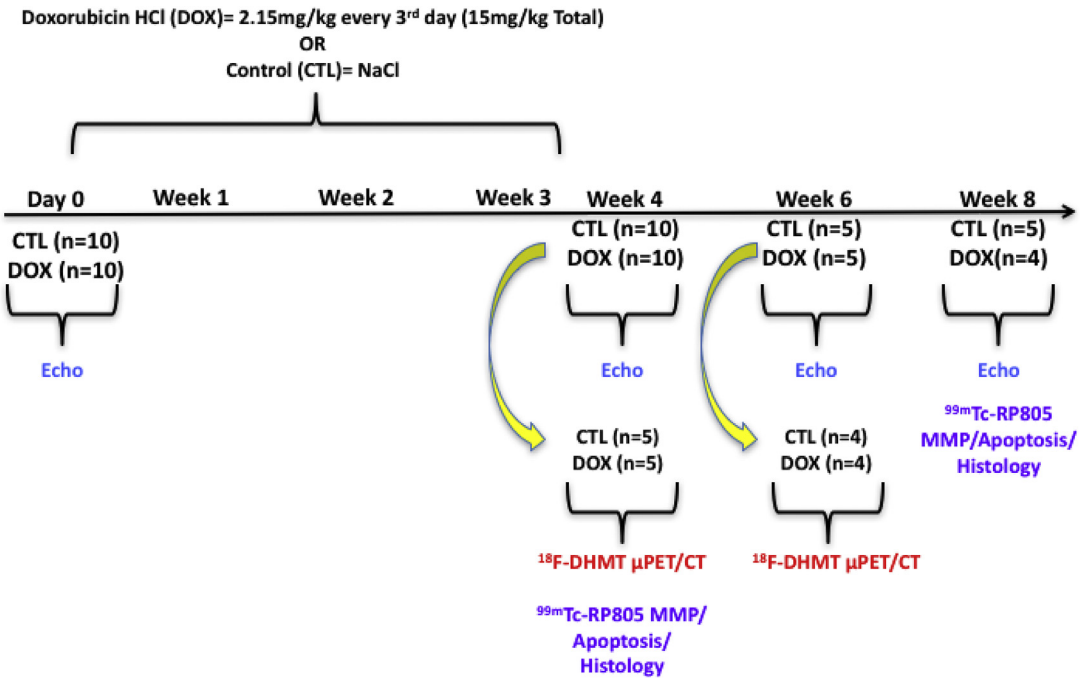

Animals were treated with either doxorubicin HCl (DOX) (15 mg/kg total, n = 10) or saline (control [CTL], n = 10) every 3 days (2.15 mg/kg/dose) for 21 days. Left ventricular function was assessed in all animals with echocardiography (echo) at baseline and 4 weeks after the initiation of DOX (n = 20). At this time, a subgroup of animals (CTL, n = 5; DOX, n = 5) were imaged with ^{18}F-DHMT positron emission tomography (PET)/computed tomography (CT). Myocardial MMP activity (^{99m}Tc-RP805), cellular cardiotoxicity and apoptosis were also assessed in these animals following euthanasia. In the remaining rats, echo (CTL, n = 5; DOX, n = 5) and ^{18}F-DHMT PET/CT (CTL, n = 4; DOX, n = 4) imaging were repeated at 6 weeks. At 8 weeks, the remaining animals (CTL, n = 5; DOX, n = 4) underwent echo imaging and evaluation of myocardial ^{99m}Tc-RP805, and histological assessment of cardiotoxicity and apoptosis following euthanasia. µPET = micro-positron emission tomography.

ROS (18). Therefore, more targeted detection of ROS activity in the heart may provide a higher sensitivity approach for detecting early cardiotoxicity that often complicates DOX therapy. Recently, a ^{18}F-labeled analog of dihydroethidium, ^{18}F-DHMT, was synthesized that permits positron emission tomographic (PET) imaging of superoxide generation in vivo (19,20). Initial studies reported an ~2-fold short-term increase in ^{18}F-DHMT cardiac uptake, indicative of elevated ROS production, in mice following a 1-time bolus injection of DOX (20 mg/kg) compared with controls (19). However, whether ^{18}F-DHMT is increased before a fall in LVEF in a more clinically relevant, progressive rodent model of DOX-induced cardiotoxicity is unknown. Taken together, we hypothesized that the novel PET radiotracer ^{18}F-DHMT would provide an early in vivo index of cardiotoxicity before a decrease in systolic function in a well-established rodent model of progressive DOX-induced cardiotoxicity.

METHODS

ANIMAL MODEL. A schematic of the overall study design is illustrated in Figure 1. Male Wistar rats (Crl:Wl) (10 to 11 weeks old) were purchased from Charles River Laboratories (Wilmington, Massachusetts) and were acclimatized to their environment for 5 days before any study procedures. All animals were housed in a temperature-controlled facility (22°C to 24°C), kept on a 12:12-h light/dark cycle, and fed a standard chow diet ad libitum for the duration of the study. We employed an established model of chronic progressive cardiotoxicity (14), in which rats were treated with DOX (2.15 mg/kg intraperitoneally every 3 days for 21 days [15 mg/kg total]) (n = 10). Control rats received an equal volume of 0.9% NaCl intraperitoneally over the same period as DOX-treated rats (n = 10). All animals were used in accordance with protocols and policies approved by the Yale Institutional Animal Care and Use Committee.

Systolic function and LV dimensions were measured with 2-dimensional (2D) echocardiography in all animals at baseline (n = 20). Four weeks following the first chemotherapy dose, cardiac function was reassessed with echocardiography (n = 20). At this time, a subgroup of control (n = 5) and DOX-treated (n = 5) animals were injected with ^{18}F-DHMT and microPET/computed tomography (CT) imaging was performed for the in vivo assessment of superoxide production. Three days following ^{18}F-DHMT microPET/CT imaging, animals were injected with ^{99m}Tc-RP805, a radiotracer that binds to the catalytic site of activated MMPs (21) for quantitative assessment of myocardial ^{99m}Tc-RP805 uptake with gamma well counting. Left ventricular tissue was harvested to assess the degree of cardiotoxicity with standard molecular and histopathologic techniques (see below). Cardiac function/dimensions (control, n = 5; DOX, n = 5) and in vivo superoxide production (control, n = 4; DOX, n = 4) were measured in the remaining animals 6 weeks following the first dose of chemotherapy with 2D echocardiography and ^{18}F-DHMT microPET/CT imaging, respectively. These animals were followed for an additional 2 weeks (8 weeks following the first dose of chemotherapy) and had cardiac function reassessed with 2D echocardiography, and had LV MMP activity and the degree of cardiotoxicity determined as described in the preceding text (control, n = 5; DOX, n = 4). One DOX-treated animal died before the last imaging session at 8 weeks.

^{18}F-DHMT SYNTHESIS. ^{18}F-DHMT was synthesized by an optimized and fully automated process developed at the Yale University PET Center as recently described (20). Further detail is provided in the Supplemental Methods. The formulated ^{18}F-DHMT product had a specific activity of 2.19 ± 0.9 mCi/nmol for the PET imaging studies.

^{18}F-DHMT microPET/CT IMAGING. Rats were injected with 0.32 ± 0.02 mCi of ^{18}F-DHMT (0.64 ± 0.004 μg injected mass) via the tail vein and underwent microPET imaging for 10 min on a dedicated small animal hybrid microPET/CT system (Inveon, Siemens Healthineers, East Walpole, Massachusetts) 60 to 70 min following tracer injection. Following microPET imaging, all animals underwent a noncontrast microCT (80 KVp, 500 μA) for attenuation correction of the PET images and to facilitate localization of radiotracer within the myocardium for quantitative image analysis. Imaging was performed under light isoflurane anesthesia (1.5% to 2.0% isoflurane/98% to 98.5% oxygen) under physiological temperatures (35.9°C to 37.5°C).

MicroPET/CT IMAGE RECONSTRUCTION, DATA CORRECTION, AND ANALYSIS. All PET images were reconstructed using a 3D ordered subset expectation maximization/maximum a posteriori algorithm with 2 ordered subset expectation maximization iterations and 18 maximization/maximum a posteriori iterations on the Siemens Inveon Acquisition Workplace. PET images were corrected for attenuation, scatter, randoms, decay, normalization, and dead time. Further detail is provided in the Supplemental Methods.

The 3D Gaussian filtering with 2-mm full-width-at-half-maximum was applied on the reconstructed images using AMIDE software (version 1.0.4) (22). In this study, the filtered PET images were only used for volumes of interest (VOIs) definition and image display, whereas the image quantification was performed on the unfiltered PET images. VOIs were drawn on the LV myocardium and within the LV cavity using the Seg3D software (version 2.1.5) (23). CT images were used to localize the heart and confirm the epicardial surfaces for VOI edge placement. Standard uptake values (SUVs) were then calculated for the LV myocardium, liver, and LV blood pool. Differences in blood pool and liver SUV were observed between groups (see later in the text); therefore, the ROS activity ratio was determined as the ratio between LV myocardial SUV and LV blood pool SUV to account for differences in tissue tracer clearance and bioavailability.

TRANSTHORACIC ECHOCARDIOGRAPHY. Transthoracic echocardiography was performed under light isoflurane anesthesia (1.5% isoflurane/98.5% oxygen) under physiological temperatures (35.9°C to 37.5°C) using standardized cardiac views and imaging modes with a high-resolution ultrasound system (Vevo 2100, VisualSonics, Toronto, Ontario, Canada) equipped with an ultra-high frequency (24 MHz) linear array transducer. LV volumes and dimensions, and systolic function were measured offline using Vevo Lab software (version 1.7.1, VisualSonics) by an experienced sonographer blinded to the treatment groups. Mitral E-A fusion was present in most rats due to tachycardia, thus diastolic function parameters were excluded from the analyses because many diastolic indices could not be accurately determined.

GAMMA WELL COUNTING OF MYOCARDIAL ^{99m}Tc-RP805 ACTIVITY. ^{99m}Tc-RP805 was used to quantify myocardial MMP activity in control (n = 5) and in DOX-treated (n = 5) rats at 4 weeks, and control (n = 5) and DOX-treated (n = 4) rats at 8 weeks following chemotherapy initiation with gamma well counting, as previously described (21,24) and described in further detail in the Supplemental Methods. Briefly, rats were injected with ~5 mCi of ^{99m}Tc- RP805 via the tail vein and were euthanized with saturated KCl 4 h following tracer injection.

^{99m}Tc-RP805 radioactivity in each tissue segment was measured by gamma well counting (Cobra Auto-Gamma, PerkinElmer, Waltham, Massachusetts) using an energy window (120 to 160 keV) centered on the peak gamma emission of ^{99m}Tc. Global LV ^{99m}Tc-RP805 uptake values are reported in percent injected dose per gram of tissue.

HISTOPATHOLOGICAL ANALYSES OF MYOCARDIUM. Paraffin embedded mid-ventricular sections (3 to 5 μm) were stained with hematoxylin and eosin (H&E) or Masson's trichrome (MT) by routine methods. H&E-stained sections were evaluated for the presence and severity of myocardial toxicity (cardiomyocyte vacuolation, degeneration) or necrosis, inflammation (histiocytic myocarditis), and MT-stained sections were evaluated for the presence and severity of myocardial fibrosis by a veterinarian (C.J.B.) trained in veterinary pathology with extensive expertise in rodent pathology, blinded to both treatment group and time point. The tissue parameters were assessed and scored using a semiquantitative criterion-based analysis adapted from prior published methods (25) as described in the Supplemental Methods. Myocardial degeneration, inflammation, and fibrosis were independently scored, and a total severity score was determined by summing the values for the 3 variables.

IMMUNOFLUORESCENCE. The terminal deoxynucleotidyl transferase-mediated nick-end labeling (TUNEL) assay was performed to assess in situ cell death according to the manufacturer's directions (Sigma-Aldrich, St. Louis, Missouri) using paraffin-embedded tissue as described in further detail in the Supplemental Methods. To ensure that nuclei were only considered for quantification, the nuclear stain DAPI (1:20,000 dilution) (ThermoFisher Scientific, Waltham, Massachusetts) was used as a counterstain according to the manufacturer's directions. In addition, the extracellular matrix antibody, anti-laminin (1:50 dilution) (Sigma-Aldrich), was used as a counterstain according to the manufacturer's directions to avoid counting cells within pericardial fat and blood vessel lumens.

Tissue sections were imaged on a fluorescent microscope (Nikon 80i, Nikon, Tokyo, Japan) and subendocardial and subepicardial fields for the anterior, septal, posterior, and lateral walls of the LV were imaged at 40× magnification for each tissue section. The number of cardiomyocytes with TUNEL-positive and DAPI costaining were counted manually per field using ImageJ software (version 1.6.0_24) (NIH, Bethesda, Maryland) (analysis grid and cell counter). The number of DAPI-stained nuclei was counted semiautomatically with a custom-developed algorithm for thresholding and segmentation (26,27) implemented in MATLAB 2017a (The MathWorks, Natick, Massachusetts). The number of TUNEL-positive cells was corrected for the number of DAPI-stained cells and multiplied by 100 to obtain a TUNEL-positive index per field. The TUNEL-positive index was then averaged over the 8 fields for subsequent statistical analysis. A biological positive control (infarct) and negative control were used to facilitate accurate TUNEL scoring.

STATISTICAL ANALYSIS. All statistical analyses were performed with SAS (version 9.4, SAS Institute, Cary, North Carolina). Longitudinal mixed-effects models were used to compare the 2 groups with respect to echocardiographic variables (LVEF, global longitudinal strain, global radial strain, LV end-diastolic volume, LV end-systolic volume, and relative wall thickness). Repeated measures models (with unstructured covariance) were used to assess the change in these parameters over time with the group and group*time interactions used as covariates. The significance level was adjusted for multiple comparisons for overall and between-group differences at each time point (0, 4, 6, 8 weeks), thus the significance level was set at $p < 0.01$ for this model. Significance is provided for between-group differences only if the overall difference in least-squares means between the groups was significant. All other data were nonparametric and not matched; thus, a Wilcoxon rank sum test was used to determine differences between groups with a significance level set a priori at $p < 0.05$. All nonparametric data are expressed as median (first quartile, third quartile). Pearson's Product Moment correlations were used to determine relationships among variables of interest with a significance level set a priori at $p < 0.05$.

RESULTS

TRANSTHORACIC ECHOCARDIOGRAPHY–DERIVED SYSTOLIC FUNCTION AND LEFT VENTRICULAR DIMENSIONS. The most widely used clinical imaging index for detection of cardiotoxicity is the LVEF, which was not significantly reduced in DOX-treated rats at 4 weeks after initiation of treatment compared with time-matched controls. Only after 6 weeks ($p = 0.0012$) and 8 weeks ($p = 0.0009$) did DOX-treated rats have a significant reduction in the LVEF compared with time-matched controls (**Figure 2A**). Similarly, global longitudinal strain, a reported index of early cardiotoxicity, only trended to be lower in DOX-treated rats at 8 weeks ($p = 0.02$) after initiation of treatment compared with time-matched controls (**Figure 2B**). Conversely, the global

FIGURE 2 Transthoracic Echocardiography–Derived Systolic Function and Ventricular Dimensions

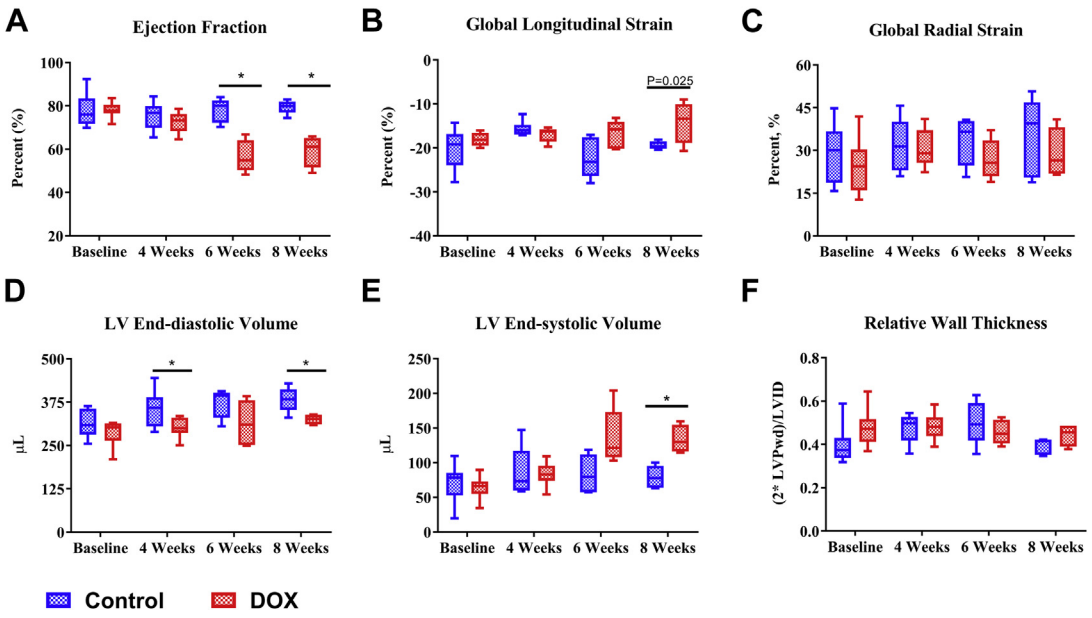

(A) Ejection fraction, **(B)** global longitudinal strain, **(C)** global radial strain, **(D)** left ventricular (LV) end-diastolic volume, **(E)** end-systolic volume, and **(F)** relative wall thickness at baseline (CTL, n = 10; DOX, n = 10), and 4 weeks (CTL, n = 10; DOX, n = 10), 6 weeks (CTL, n = 5; DOX, n = 5), and 8 weeks (CTL, n = 5; DOX, n = 4) following the initiation of chemotherapy in DOX-treated rats and time-matched controls. *p < 0.01 between-group difference. **Box plots** display the median **(horizontal bar)**, first quartile, third quartile, and minimum and maximum values **(whiskers)**. LVPwd = left ventricular posterior wall thickness at end-diastole; LVID = left ventricular internal diameter; other abbreviations as in Figure 1.

radial strain, another reported early index of cardiotoxicity, was not significantly different between the groups overall or at any time point (Figure 2C).

LV end-diastolic volumes were significantly different between control and DOX-treated rats at 4 weeks (p = 0.0108) and 8 weeks (p = 0.006) (Figure 2D). In addition, LV end-diastolic volumes in DOX-treated rats trended lower than controls at 6 (p = 0.048) (Figure 2D). Aligned with the LVEF changes, LV end-systolic volume trended to increase at 6 weeks (p = 0.052) and was significantly increased at 8 weeks after the initiation of DOX treatment compared with time-matched controls (p = 0.0006) (Figure 2E). DOX treatment did not influence relative wall thickness (2 × posterior wall thickness/LV internal diameter) overall or at any time point compared with controls (Figure 2F).

MicroPET/CT ^{18}F-DHMT IMAGING OF IN VIVO MYOCARDIAL ROS PRODUCTION. Representative ^{18}F-DHMT microPET/CT images of each experimental group are shown in Figure 3A. The myocardium-to-blood ROS SUV ratio was 35% higher in DOX-treated animals compared with time-matched controls at 4 weeks after initiation of treatment (p = 0.03), before any decrease in the LVEF (Figure 3B). At 6 weeks, this ratio was 56% higher in DOX-treated animals compared with time-matched controls (p = 0.03). Interestingly, we observed a modest inverse correlation (r^2 = 0.65; p = 0.01) between ejection fraction and in vivo myocardial ROS production at 6 weeks in DOX-treated rats (n = 4) and matched controls (n = 4) (Figure 3C), suggesting that the magnitude of the decline in LV function is associated with an increase in myocardial ROS production. Similarly, LV end-systolic volume was modestly and directly correlated (r^2 = 0.72; p = 0.007) with ^{18}F-DHMT uptake in these rats (Figure 3D).

LV, liver, and blood SUV values for DOX-treated animals (and time-matched controls) at 4 and 6 weeks after DOX initiation are shown in Supplemental Table 1. At 4 weeks post-DOX initiation, the LV SUV tended to be lower in the DOX-treated animals compared with time-matched controls (p = 0.06), whereas both liver (p = 0.007) and blood pool (p = 0.03) SUVs were significantly lower in the DOX-treated animals compared with controls at this time. At 6 weeks post-DOX initiation, there were no differences in the LV SUV between

FIGURE 3 ^{18}F-DHMT microPET/CT Imaging and Quantitation of the Myocardial ROS Activity Ratio

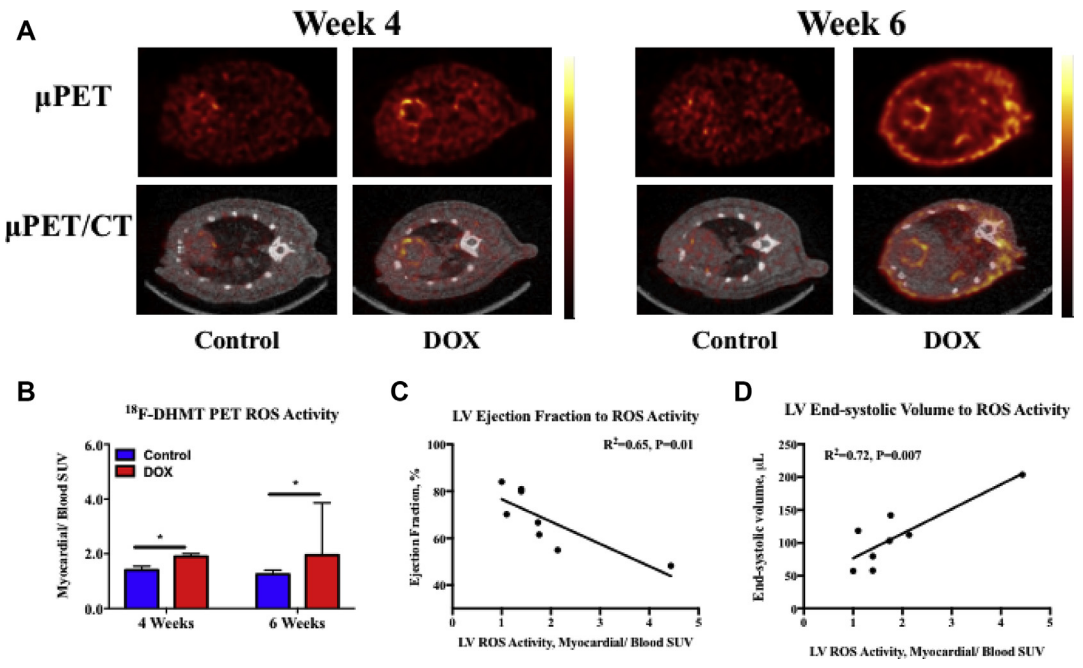

(A) Representative micro/PET **(top row)** and fused microPET/CT **(bottom row)** images following ^{18}F-DHMT injection from a control and a matched DOX-treated rat imaged at 4 weeks after chemotherapy initiation **(left)**, and a control and corresponding DOX-treated rat imaged at 6 weeks following chemotherapy initiation **(right)**. Each individual image is scaled to the blood pool SUV. **(B)** Quantified myocardial-to-blood pool SUV ratios between controls (n = 5) and DOX-treated rats (n = 5) at 4 weeks, and controls (n = 4) and DOX-treated rats (n = 4) at 6 weeks following chemotherapy initiation. **(C)** Correlation between LVEF and LV ^{18}F-DHMT uptake (myocardial-to-blood pool SUV), and **(D)** between LV end-systolic volume and LV ^{18}F-DHMT uptake (myocardial-to-blood pool SUV) in DOX-treated rats at 6 weeks (n = 4) and matched controls (n = 4). *p < 0.05 between-group difference. Values are expressed as median with interquartile range. LVEF = left ventricular ejection fraction; ROS = reactive oxygen species; SUV = standardized uptake value; other abbreviations as in Figures 1 and 2.

DOX-treated animals and time-matched controls (p = 0.34), whereas liver ^{18}F-DHMT uptake was significantly lower in DOX-treated animals compared with controls (p = 0.03). At this time, blood pool SUVs also tended to be lower in the DOX-treated rats compared with controls (p = 0.06).

MYOCARDIAL ^{99m}Tc-RP805 ACTIVITY. Temporal changes in the retention of ^{99m}Tc-RP805 in the myocardium of the LV, which reflect myocardial MMP activity, are shown in Figure 4A for control and DOX-treated rats. At 4 weeks, ^{99m}Tc-RP805 retention was nonsignificantly elevated in DOX-treated rats compared with time-matched controls (p = 0.056). However, at 8 weeks, ^{99m}Tc-RP805 retention was significantly increased in DOX-treated rats compared with time-matched controls (p = 0.01) and to DOX-treated rats at 4 weeks (p = 0.01).

In 8-week rats, we correlated LV systolic function and dimensions with MMP activity to assess the relationship between changes in LV function and volumes to elevations in MMP activity. We observed a modest inverse linear correlation (r^2 = 0.67; p = 0.01) between ejection fraction and ^{99m}Tc-RP805 uptake in DOX-treated rats (n = 4) at 8 weeks and matched controls (n = 5) (Figure 4B), suggesting that a decline in LV function is associated with increased myocardial MMP activity. Similarly, LV end-systolic volume had a direct linear correlation (r^2 = 0.63; p = 0.02) with ^{99m}Tc-RP805 uptake in these rats (Figure 4C).

HISTOPATHOLOGY. Blinded review of H&E- and MT-stained tissue confirmed graded cardiotoxicity associated with this rat model. As expected, control rats displayed no significant pathological findings. Aligned with the model, DOX-treated rats euthanized at 4 weeks had a nonsignificantly greater overall severity score compared with time-matched control rats (p = 0.08) with some evidence of fibrosis, inflammation, and myocardial degeneration. DOX-treated rats euthanized at 8 weeks following chemotherapy initiation had more progressive fibrosis, focal myocardial inflammation, and myocardial vacuolation (degeneration) contributing to a nonsignificantly

FIGURE 4 LV ^{99m}Tc-RP805 Uptake

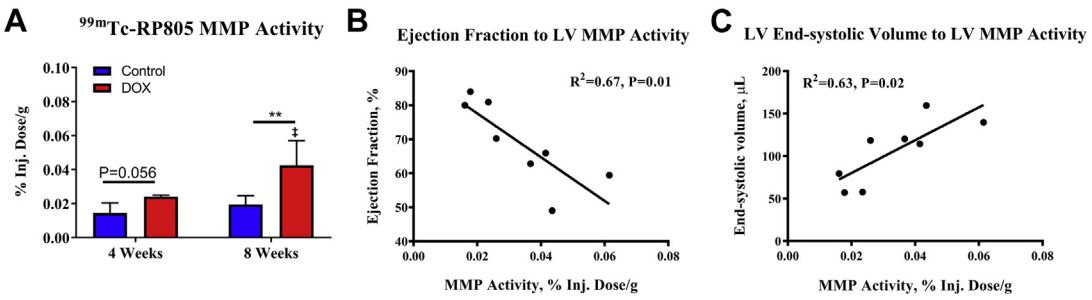

(A) LV ^{99m}Tc-RP805 uptake between controls (n = 5) and DOX-treated rats (n = 5) at 4 weeks, and controls (n = 5) and DOX-treated rats (n = 4) 8 weeks following chemotherapy initiation. Correlation between **(B)** LV ejection fraction and LV ^{99m}Tc-RP805 uptake, and **(C)** LV end-systolic volume and LV ^{99m}Tc-RP805 uptake in DOX-treated rats at 8 weeks (n = 4) and matched controls (n = 5). **p = 0.01 between-group difference. ‡p < 0.05 within-group difference compared with 4-week rats. Values are expressed as median with interquartile range. Inj. = injected; MMP = matrix metalloproteinase; other abbreviations as in Figures 1 to 3.

elevated overall severity score compared with DOX-treated rats at 4 weeks and a significantly elevated overall severity score compared with time-matched controls (p = 0.02) (Figure 5).

CELLULAR APOPTOSIS. Representative fluorescent images for laminin, DAPI, and TUNEL stains, and a merged image of these 3 stains are shown in Figures 6A to 6D from a DOX-treated rat at 8 weeks. The results of the quantitative analysis of TUNEL-positive staining for all rats is shown in Figure 6E. Unlike the observed progressive histopathologic changes described in the preceding text, cellular apoptosis only trended to increase in DOX-treated rats at 8 weeks compared with time-matched controls rats (p = 0.06) and was significantly increased compared with DOX-treated rats at 4 weeks (p < 0.02) (Figure 6E).

DISCUSSION

The major finding from the present study is that ^{18}F-DHMT, a novel ROS-targeted PET radiotracer, was able to noninvasively detect an early elevation in myocardial in vivo ROS production before a fall in the LVEF in an established rodent model of progressive DOX-induced cardiotoxicity. The early elevation in myocardial ROS production was associated with only mild histologic evidence of myocardial toxicity and occurred before any significant activation of myocardial remodeling enzymes (e.g., MMP activity) or cellular apoptosis compared with controls. Other more sensitive echocardiographic indices of systolic function were also unchanged at this time of early ROS activation. It is important to note that the subsequent drop in LVEF, which occurred over time in DOX-treated rats, was associated with a significant increase in myocardial degeneration, MMP activation, and cellular apoptosis. Thus, decline in LVEF, which is typically used clinically for detection of cardiotoxicity, occurs at a point where irreversible myocardial injury has already occurred.

DOX has been shown to increase ROS levels through multiple pathways including, but not limited to, mitochondrial redox cycling of iron-doxorubicin complexes (28), activation of the renin-angiotensin-aldosterone system (29), increased expression of nicotinamide adenine dinucleotide phosphate (NADPH) oxidases (30), and changes in the mitochondrial and nuclear transcriptome (31). In addition, DOX decreases reduced gluthathione levels and decreases catalase activity, thus impairs the inherent cardiac antioxidant defense system (11). The ROS-dependent cardiotoxic effects of DOX are numerous and include apoptosis through direct DNA damage (11,12), a reduction in mitochondrial function (32), increased fibrosis and remodeling through direct activation and increased expression of MMPs (13,14), up-regulation of the proinflammatory pathways (12), and altered excitation-contraction coupling through impairing calcium dynamics (33). It appears that excessive ROS production is a key upstream event in DOX-induced cardiotoxicity, because numerous studies report an improvement or reversal of cardiotoxicity with antioxidant therapy (34–36) or direct manipulation of key molecular targets in ROS producing or quenching pathways (11,12,30,37). Our findings extend these prior observations, because we show that in vivo cardiac ROS production with ^{18}F-DHMT PET/CT imaging precedes the impairment in cardiac function often associated with DOX-induced cardiotoxicity. Notably, a

FIGURE 5 Histopathology Score

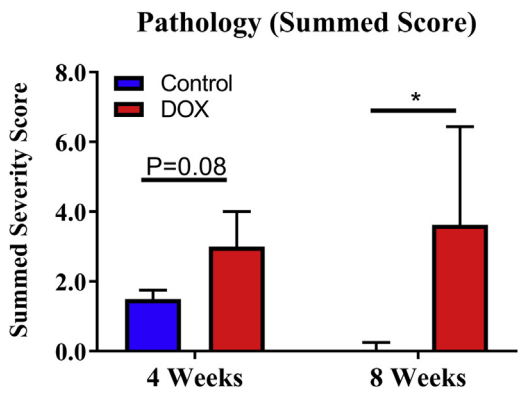

Quantified cardiotoxicity grading (summed severity score) between controls (n = 5) and doxorubicin (DOX)-treated rats (n = 5) at 4 weeks, and controls (n = 5) and DOX-treated rats (n = 4) 8 weeks following chemotherapy initiation. *p < 0.05 between-group difference. Values are expressed as median with interquartile range.

separate, independently acting mechanism of DOX-induced cardiotoxicity has been proposed that describes DOX binding to topoisomerase-2β and DNA as a trigger of cell death and transcriptome changes that secondarily lead to excessive ROS formation (31). Our findings of increased in vivo cardiac ROS production before cellular apoptosis are inconsistent with these reports; however, it is unclear at this time how specific pathways that lead to cardiotoxicity may predominate, when they may be activated, and how they may interact. Differences in chemotherapy dosing and animal models may also account for discordance between studies.

Accumulating preclinical evidence suggests that activation of several MMP isoforms (MMP-1, -2, -9, -14) play a key role in acute and chronic DOX cardiotoxicity by contributing to myocardial fibrosis, collagen disorganization, and contractile dysfunction (13,14). Here, we observed an elevation in myocardial MMP activity in DOX-treated rats observed at a later time point following DOX therapy (8 weeks), but not in DOX-treated animals observed at an earlier time point (4 weeks) compared with controls. In addition, we observed a modest correlation between systolic dysfunction and myocardial MMP activity in DOX-treated rats at 8 weeks and matched controls. In agreement with other studies (14,38,39), our data suggest that ROS production may lead to activation of myocardial MMPs, and that MMP activation contributes, at least in part, to LV remodeling and dysfunction. However, we cannot rule out the possibility that factors other than elevated ROS production contributed to MMP activation observed in this model.

Several noninvasive imaging modalities have been proposed for early detection and prediction of cardiotoxicity. Preclinical and clinical reports indicate the use of myocardial deformation (e.g., global longitudinal strain) imaging with echocardiography, although the high technical variability of these methods and nonstandardized analysis packages have led to inconsistent support of these functional indices (6). Similarly, perturbations in some echocardiographic indices of diastolic function, such as prolonged isovolumic relaxation time, reduced mitral inflow velocity, a reduction in mitral inflow velocity/atrial flow velocity, and a reduction in mitral inflow velocity deceleration time have been shown to precede changes in systolic function after anthracycline treatment (40-42). However, the poor reproducibility of these echocardiographic indices of diastolic function has limited their application as early indicators of anthracycline-induced cardiotoxicity (4). Magnetic resonance imaging has also been applied for evaluation of early myocardial edema and/or inflammation (T2-weighted imaging) and early cardiac fibrosis/extracellular volume changes (T1-weighted imaging) in the setting of cardiotoxic chemotherapy agents (10,43); however, the utility of these magnetic resonance indices remains controversial due to conflicting reports (43,44).

A few studies have proposed radiotracer-based molecular imaging methods as highly sensitive diagnostic tools for early detection of cardiotoxicity, because these methods are able to directly target molecular (apoptosis, ^{99m}Tc-annexin V), metabolic (fatty acid oxidation, ^{123}I-beta-methyl-p-iodo-phenyl-pentadecanoic acid), and physiological (sympathetic denervation, ^{123}I-metaiodobenzylguanidine) alterations associated with the underlying disease pathophysiology and progression (45-47). Along these lines, we hypothesized that ^{18}F-DHMT PET imaging of in vivo ROS production may be valuable for early detection of DOX-induced cardiotoxicity, because increased ROS production plays a critical role in DOX-induced cardiotoxicity. In accordance with this hypothesis, we show for the first time to our knowledge, that ^{18}F-DHMT imaging was able to detect an early elevation in cardiac ROS production before a fall in ejection fraction in a progressive rodent model of DOX-induced cardiotoxicity. These findings extend initial studies that reported an ~2-fold increase in ^{18}F-DHMT cardiac uptake compared with controls following a 1-time bolus injection of DOX (20 mg/kg) in mice (19). As compared with that acute model, the chronic model used in the current work more adequately resembles clinically observed anthracycline-induced

FIGURE 6 TUNEL Staining and Quantitation of Cellular Apoptosis

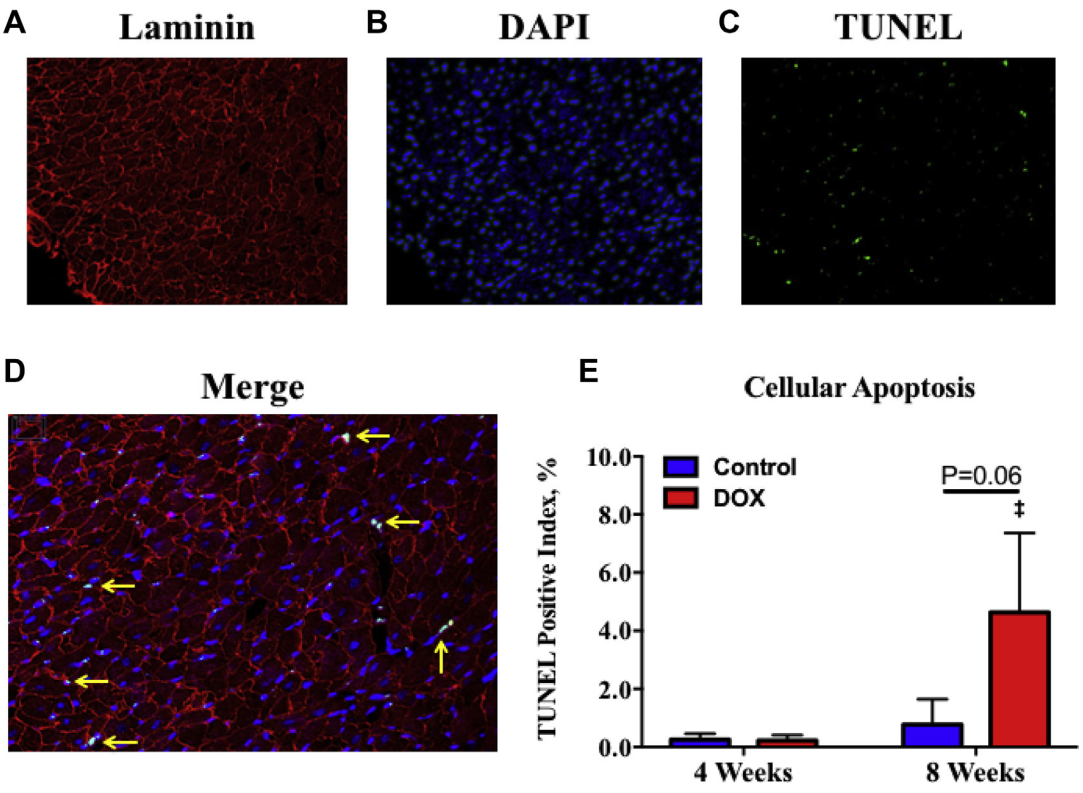

(A) Representative laminin, **(B)** DAPI, **(C)** TUNEL, and **(D)** a merged image of these 3 stains from a doxorubicin (DOX)-treated rat at 8 weeks following chemotherapy initiation. **Yellow arrows** point to nuclei costained with DAPI and TUNEL that were considered positive. **(B)** Quantified TUNEL-positive nuclei per 40× field (average over subendocardial and subepicardial fields for the lateral, septal, inferior, and lateral walls) between controls (n = 5) and DOX-treated rats (n = 5) at 4 weeks, and controls (n = 5) and DOX-treated rats (n = 4) 8 weeks following chemotherapy initiation. **(E)** ‡$p < 0.05$ within-group difference compared with 4-week rats. Values are expressed as median with interquartile range. TUNEL = terminal deoxynucleotidyl transferase-mediated nick-end labeling.

cardiotoxicity, which manifests as LV systolic dysfunction, is progressive, and typically occurs after completion of chemotherapy (4).

STUDY LIMITATIONS. First, ^{18}F-DHMT oxidation and subsequent cellular retention largely reflect superoxide activity. Therefore, the utility of measuring other ROS, such as hydrogen peroxide with peroxy-caged-[^{18}F]fluorodeoxy thymidine-1 (PC-^{18}F-FLT-1) (48) or redox status with 1-[C^{11}]methyl-1,4-dihydroquinoline-3-carboxamide (^{11}C-DHQ1) (49) using PET/CT for early detection of DOX-induced cardiotoxicity is unknown. However, a large portion of cardiac ROS produced during DOX therapy arises from the mitochondria and NADPH oxidases, both sources of superoxide (30,37), thus supporting the use and early rise of cardiac ^{18}F-DHMT uptake observed in this model. Second, it is possible that DOX influences ^{18}F-DHMT myocardial kinetics, peripheral tissue uptake and metabolism, and tracer clearance. Thus, SUV measurements presented herein only provide a semiquantitative assessment of myocardial ^{18}F-DHMT retention and superoxide production in this complex model. Observed changes in the bioavailability of the tracer between groups were addressed by correcting the LV SUV to the blood SUV, which is appropriate for tracers that can be best characterized by a 2-tissue irreversible kinetic model. Because ^{18}F-DHMT oxidation within the myocardium is irreversible, the trend of ROS in response to chemotherapy based on our calculation of myocardium-to-blood pool SUV ratio is appropriate to account for potential confounding factors in the blood and is expected to be directly proportional to quantification parameters (e.g., K_i) derived from the kinetic analysis in dynamic PET. For example, a recent ^{18}F-FDG study reported that the ratio of tumor SUV to blood SUV derived from static PET had a much stronger

correlation with the retention index K_i derived from dynamic PET with kinetic modeling, when compared with tumor SUV alone, because the SUV ratio reduced the residual interstudy variability of the input function in the SUV calculation (50). Ultimately, full compartmental modeling with an arterial input function and high-performance liquid chromatography analysis of blood and tissue metabolites will be needed to absolutely quantify myocardial ^{18}F-DHMT retention and superoxide production, although this approach will be most effectively accomplished in larger animals and humans. Third, we were unable to accurately quantify diastolic function in these animal's due to E-A wave fusion, thus we cannot exclude the possibility that diastolic dysfunction may have preceded systolic dysfunction in this model. Therefore, it is unknown at this time whether ^{18}F-DHMT PET imaging would out perform this echocardiographic index of early anthracycline-induced cardiotoxicity. Finally, the specific molecular pathways that led to the increase in cardiac superoxide production were not addressed in this study, and are beyond the scope of this study. However, measuring global superoxide production with ^{18}F-DHMT is valuable for diagnostic and predictive applications in the early assessment of DOX-induced cardiotoxicity and potentially other disease processes involving ROS activation, because superoxide produced from all pathways contributes to aberrant cell signaling and damage/death.

CONCLUSIONS

^{18}F-DHMT PET/CT imaging was able to noninvasively detect an early elevation in myocardial ROS production in vivo, before a fall in LVEF in an established chronic rodent model of progressive DOX-induced cardiotoxicity. Importantly, this early elevation in myocardial ROS was associated with only mild myocardial toxicity, and no significant changes in MMP activity or cellular apoptosis. On the other hand, a fall in the LVEF was associated with higher levels of ROS production, more advanced myocardial toxicity, activation of myocardial MMPs, and cellular apoptosis. These preliminary data suggest that ^{18}F-DHMT PET/CT imaging may allow for early assessment of cardiotoxicity that precedes the often-irreversible decline in systolic function in cancer patients receiving DOX. Future investigations should focus on evaluating the ability of ^{18}F-DHMT PET/CT imaging to predict changes in systolic dysfunction with DOX therapy and evaluate therapeutic interventions to limit cardiotoxicity in order to fully elucidate the clinical potential of this ROS-targeted radiotracer.

ACKNOWLEDGMENTS The authors gratefully acknowledge the technical assistance of Nicole Mikush and Xiangning Wang of the Yale Translational Research Imaging Center, along with the technical staff at the Yale PET Center.

ADDRESS FOR CORRESPONDENCE: Dr. Albert J. Sinusas, Section of Cardiovascular Medicine, Yale University School of Medicine, P.O. Box 208017, Dana 3, New Haven, Connecticut 06520-8017. E-mail: albert.sinusas@yale.edu.

PERSPECTIVES

COMPETENCY IN MEDICAL KNOWLEDGE 1: Doxorubicin is an effective chemotherapy agent but is associated with cardiotoxicity. Current noninvasive screening methods for doxorubicin-induced cardiotoxicity are based on the serial assessment of the LVEF. However, the measurement of LVEF is variable and unable to detect cardiotoxicity before overt, non-reversible myocardial toxicity. Decades of basic science research have indicated that ROS are key mediators in doxorubicin-induced cardiotoxicity. Our study provides evidence that PET/computed tomography imaging of ^{18}F-DHMT, a marker of superoxide production, allows for early detection of cardiotoxicity in rodents, and that the early elevation in myocardial ^{18}F-DHMT uptake occurs before decrements in LVEF and overt myocardial toxicity following doxorubicin administration.

COMPETENCY IN MEDICAL KNOWLEDGE 2: Assessment of myocardial superoxide production can be achieved noninvasively using PET imaging of ^{18}F-DHMT. The application of this technique in cancer patients receiving doxorubicin or other anthracyclines may facilitate the early detection of cardiotoxicity, thereby helping to guide optimal oncological treatment and avoid cardiotoxicity.

TRANSLATIONAL OUTLOOK: Studies in large animal models of anthracycline-induced cardiotoxicity and in cancer patients receiving anthracycline chemotherapy are warranted to determine the potential clinical utility of ^{18}F-DHMT PET imaging for early detection of cardiotoxicity. The ability to detect in vivo myocardial superoxide production with ^{18}F-DHMT PET imaging also provides the opportunity to apply this tracer in other cardiovascular diseases in which excessive production of ROS contributes to disease progression.

REFERENCES

1. Yeh ET, Bickford CL. Cardiovascular complications of cancer therapy: incidence, pathogenesis, diagnosis, and management. J Am Coll Cardiol 2009;53:2231–47.

2. Swain SM, Whaley FS, Ewer MS. Congestive heart failure in patients treated with doxorubicin: a retrospective analysis of three trials. Cancer 2003;97:2869–79.

3. Von Hoff DD, Layard MW, Basa P, et al. Risk factors for doxorubicin-induced congestive heart failure. Ann Intern Med 1979;91:710–7.

4. Russell RR, Alexander J, Jain D, et al. The role and clinical effectiveness of multimodality imaging in the management of cardiac complications of cancer and cancer therapy. J Nucl Cardiol 2016;23:856–84.

5. Ewer MS, Ali MK, Mackay B, et al. A comparison of cardiac biopsy grades and ejection fraction estimations in patients receiving adriamycin. J Clin Oncol 1984;2:112–7.

6. Thavendiranathan P, Poulin F, Lim K-D, Plana JC, Woo A, Marwick TH. Use of myocardial strain imaging by echocardiography for the early detection of cardiotoxicity in patients during and after cancer chemotherapy: a systematic review. J Am Coll Cardiol 2014;63:2751–68.

7. Cardinale D, Colombo A, Lamantia G, et al. Anthracycline-induced cardiomyopathy: clinical relevance and response to pharmacologic therapy. J Am Coll Cardiol 2010;55:213–20.

8. Ky B, Putt M, Sawaya H, et al. Early increases in multiple biomarkers predict subsequent cardiotoxicity in patients with breast cancer treated with doxorubicin, taxanes, and trastuzumab. J Am Coll Cardiol 2014;63:809–16.

9. Serrano JM, Gonzalez I, Del Castillo S, et al. Diastolic dysfunction following anthracycline-based chemotherapy in breast cancer patients: incidence and predictors. Oncologist 2015;20:864–72.

10. Vasu S, Hundley WG. Understanding cardiovascular injury after treatment for cancer: an overview of current uses and future directions of cardiovascular magnetic resonance. J Cardiovasc Magn Reson 2013;15:66.

11. Mukhopadhyay P, Rajesh M, Batkai S, et al. Role of superoxide, nitric oxide, and peroxynitrite in doxorubicin-induced cell death in vivo and in vitro. Am J Physiol Heart Circ Physiol 2009;296:H1466–83.

12. Wang S, Kotamraju S, Konorev E, Kalivendi S, Joseph J, Kalyanaraman B. Activation of nuclear factor-kappaB during doxorubicin-induced apoptosis in endothelial cells and myocytes is pro-apoptotic: the role of hydrogen peroxide. Biochem J 2002;367:729–40.

13. Polegato BF, Minicucci MF, Azevedo PS, et al. Acute doxorubicin-induced cardiotoxicity is associated with matrix metalloproteinase-2 alterations in rats. Cell Physiol Biochem 2015;35:1924–33.

14. Ivanova M, Dovinova I, Okruhlicova L, et al. Chronic cardiotoxicity of doxorubicin involves activation of myocardial and circulating matrix metalloproteinases in rats. Acta Pharmacol Sin 2012;33:459–69.

15. Putt M, Hahn VS, Januzzi JL, et al. Longitudinal changes in multiple biomarkers are associated with cardiotoxicity in breast cancer patients treated with doxorubicin, taxanes, and trastuzumab. Clin Chem 2015;61:1164–72.

16. Gilliam LA, Fisher-Wellman KH, Lin C-T, Maples JM, Neufer PD. Doxorubicin impairs skeletal muscle mitochondrial respiratory capacity in skeletal muscle. FASEB J 2012;26:1144. 8.

17. Kalender Y, Yel M, Kalender S. Doxorubicin hepatotoxicity and hepatic free radical metabolism in rats: the effects of vitamin E and catechin. Toxicology 2005;209:39–45.

18. Pelicano H, Carney D, Huang P. ROS stress in cancer cells and therapeutic implications. Drug Resist Updat 2004;7:97–110.

19. Chu W, Chepetan A, Zhou D, et al. Development of a PET radiotracer for non-invasive imaging of the reactive oxygen species, superoxide, in vivo. Org Biomol Chem 2014;12:4421–31.

20. Zhang W, Cai Z, Li L, et al. Optimized and automated radiosynthesis of [18F] DHMT for translational imaging of reactive oxygen species with positron emission tomography. Molecules 2016;21:1696.

21. Su H, Spinale FG, Dobrucki LW, et al. Noninvasive targeted imaging of matrix metalloproteinase activation in a murine model of postinfarction remodeling. Circulation 2005;112:3157–67.

22. Loening AM, Gambhir SS. AMIDE: a free software tool for multimodality medical image analysis. Mol Imaging 2003;2:131–7.

23. Seg3D: volumetric image segmentation and visualization (Software). Scientific Computing and Imaging Institute (SCI) (2015) Available at: http://www.seg3d.org. Accessed March 2018.

24. Sahul ZH, Mukherjee R, Song J, et al. Targeted imaging of the spatial and temporal variation of matrix metalloproteinase activity in a porcine model of postinfarct remodeling relationship to myocardial dysfunction. Circ Cardiovasc Imaging 2011;4:381–91.

25. Montgomery RR, Booth CJ, Wang X, Blaho VA, Malawista SE, Brown CR. Recruitment of macrophages and polymorphonuclear leukocytes in Lyme carditis. Infect Immun 2007;75:613–20.

26. Otsu N. A threshold selection method from gray-level histograms. IEEE Trans Syst Man Cybern Syst 1979;9:62–6.

27. Meyer F. Topographic distance and watershed lines. Signal processing 1994;38:113–25.

28. Rochette L, Guenancia C, Gudjoncik A, et al. Anthracyclines/trastuzumab: new aspects of cardiotoxicity and molecular mechanisms. Trends Pharmacol Sci 2015;36:326–48.

29. Toko H, Oka T, Zou Y, et al. Angiotensin II type 1a receptor mediates doxorubicin-induced cardiomyopathy. Hypertgens Res 2002;25:597–603.

30. Zhao Y, McLaughlin D, Robinson E, et al. Nox2 NADPH oxidase promotes pathologic cardiac remodeling associated with Doxorubicin chemotherapy. Cancer Res 2010;70:9287–97.

31. Zhang S, Liu X, Bawa-Khalfe T, et al. Identification of the molecular basis of doxorubicin-induced cardiotoxicity. Nat Med 2012;18:1639–42.

32. Clementi ME, Giardina B, Di Stasio E, Mordente A, Misiti F. Doxorubicin-derived metabolites induce release of cytochrome C and inhibition of respiration on cardiac isolated mitochondria. Anticancer Res 2003;23:2445–50.

33. Timolati F, Ott D, Pentassuglia L, et al. Neuregulin-1 beta attenuates doxorubicin-induced alterations of excitation-contraction coupling and reduces oxidative stress in adult rat cardiomyocytes. J Mol Cell Cardiol 2006;41:845–54.

34. Dong Q, Chen L, Lu Q, et al. Quercetin attenuates doxorubicin cardiotoxicity by modulating Bmi-1 expression. Brit J Pharmcol 2014;171:4440–54.

35. Chandran K, Aggarwal D, Migrino RQ, et al. Doxorubicin inactivates myocardial cytochrome c oxidase in rats: cardioprotection by Mito-Q. Biophys J 2009;96:1388–98.

36. Seifert CF, Nesser ME, Thompson DF. Dexrazoxane in the prevention of doxorubicin-induced cardiotoxicity. Ann Pharmacother 1994;28:1063–72.

37. Ichikawa Y, Ghanefar M, Bayeva M, et al. Cardiotoxicity of doxorubicin is mediated through mitochondrial iron accumulation. J Clin Invest 2014;124:617–30.

38. Spallarossa P, Altieri P, Garibaldi S, et al. Matrix metalloproteinase-2 and-9 are induced differently by doxorubicin in H9c2 cells: the role of MAP kinases and NAD (P) H oxidase. Cardiovasc Res 2006;69:736–45.

39. Siwik DA, Colucci WS. Regulation of matrix metalloproteinases by cytokines and reactive oxygen/nitrogen species in the myocardium. Heart Fail Rev 2004;9:43–51.

40. Tassan-Mangina S, Codorean D, Metivier M, et al. Tissue Doppler imaging and conventional echocardiography after anthracycline treatment in adults: early and late alterations of left ventricular function during a prospective study. Eur J Echocardiogr 2006;7:141–6.

41. Marchandise B, Schroeder E, Bosly A, et al. Early detection of doxorubicin cardiotoxicity: interest of Doppler echocardiographic analysis of left ventricular filling dynamics. Am Heart J 1989;118:92–8.

42. Stoddard MF, Seeger J, Liddell NE, Hadley TJ, Sullivan DM, Kupersmith J. Prolongation of isovolumetric relaxation time as assessed by Doppler echocardiography predicts doxorubicin-induced systolic dysfunction in humans. J Am Coll Cardiol 1992;20:62–9.

43. Jordan JH, D'Agostino RB Jr., Hamilton CA, et al. Longitudinal assessment of concurrent changes in left ventricular ejection fraction and left ventricular myocardial tissue characteristics after administration

of cardiotoxic chemotherapies using T1-weighted and T2-weighted cardiovascular magnetic resonance. Circ Cardiovasc Imaging 2014;7:872–9.

44. Neilan TG, Coelho-Filho OR, Pena-Herrera D, et al. Left ventricular mass in patients with a cardiomyopathy after treatment with anthracyclines. Am J Cardiol 2012;110:1679–86.

45. Bennink RJ, van den Hoff MJ, van Hemert FJ, et al. Annexin V imaging of acute doxorubicin cardiotoxicity (apoptosis) in rats. J Nucl Med 2004;45:842–8.

46. Carrió I, Estorch M, Berná L, Lopez-Pousa J, Tabernero J, Torres G. Indium-111-antimyosin and iodine-123-MIBG studies in early assessment of doxorubicin cardiotoxicity. J Nucl Med 1995;36:2044–9.

47. Saito K, Takeda K, Okamoto S, et al. Detection of doxorubicin cardiotoxicity by using iodine-123 BMIPP early dynamic SPECT: quantitative evaluation of early abnormality of fatty acid metabolism with the Rutland method. J Nucl Cardiol 2000;7:553–61.

48. Carroll V, Michel BW, Blecha J, et al. A boronate-caged [18F] FLT probe for hydrogen peroxide detection using positron emission tomography. J Am Chem Soc 2014;136:14742–5.

49. Okamura T, Okada M, Kikuchi T, Wakizaka H, Zhang M-R. A 11C-labeled 1, 4-dihydroquinoline derivative as a potential PET tracer for imaging of redox status in mouse brain. J Cereb Blood Flow Metab 2015;35:1930–6.

50. van den Hoff J, Oehme L, Schramm G, et al. The PET-derived tumor-to-blood standard uptake ratio (SUR) is superior to tumor SUV as a surrogate parameter of the metabolic rate of FDG. EJNMMI Res 2013;3:77.

KEY WORDS cardiotoxicity, doxorubicin, positron emission tomography, reactive oxygen species

APPENDIX For an expanded Methods section as well as a supplemental table, please see the online version of this paper.